

Optical evidence for bonding-antibonding splitting in IrTe₂

D. Mazumdar,¹ K. Haule,² J. J. Yang,³ G. L. Pascut,² B. S. Holinsworth,¹ K. R. O'Neal,¹ V. Kiryukhin,^{2,4} Sang-Wook Cheong,^{2,3,4} and J. L. Musfeldt¹

¹Department of Chemistry, University of Tennessee, Knoxville, Tennessee 37996, USA

²Department of Physics and Astronomy, Rutgers University, Piscataway, New Jersey 08854, USA

³Laboratory for Pohang Emergent Materials and Department of Physics, Pohang University of Science and Technology, Pohang 790-784, Korea

⁴Rutgers Center for Emergent Materials, Rutgers University, Piscataway, New Jersey 08854, USA

(Received 21 May 2014; revised manuscript received 22 November 2014; published 7 January 2015)

We combined optical spectroscopy with first principles calculations to reveal the electronic signatures of Ir dimer formation in the $q = (1/5, 0, 1/5)$ high resistivity phase of IrTe₂. Our measurements uncover two interband transitions into the unoccupied d_{xy} antibonding orbital, one from mixed iridium/tellurium bands, the other from the d_{xy} bonding orbital of the dimerized Ir centers. The bonding-antibonding splitting demonstrates that iridium, not tellurium, plays the dominant role in stabilizing the low temperature phase of IrTe₂ through localized bonding orbital formation.

DOI: [10.1103/PhysRevB.91.041105](https://doi.org/10.1103/PhysRevB.91.041105)

PACS number(s): 78.20.-e, 71.15.Mb, 77.84.Bw

IrTe₂ has received significant attention due to its intriguing structural transition at 280 K to a high resistance phase characterized by a wave vector $q = (1/5, 0, 1/5)$ [1–3]. This transition has been hard to classify. It was thought to be driven by a Peierls instability [1], similar to other layered metal dichalcogenides [4,5], but experiments show no evidence for a charge density wave gap [6,7]. Therefore, effort has been devoted to understanding the transition in terms of the mixed-valent, bonding, and orbital properties of Ir and Te [8–10]. Recently, x-ray diffraction measurements on IrTe₂ single crystals revealed the presence of Ir dimers in the 1/5 unit cell (Fig. 1) [11,12]. Further first principles density functional theory (DFT) and dynamic mean field theory (DMFT) calculations confirm that the dimerization does not lead to a gap, but to a reduced density of states at the Fermi level [11,12]. Even more intriguing is the observation of additional domain modulations (1/6, 1/8, 1/11) below 180 K from scanning tunneling microscopy [13]. Doping suppresses the 1/5th phase, leading instead to low temperature superconductivity [1,7,14].

In this combined experimental-theoretical effort, we provide clear optical evidence for Ir dimerization in the 1/5th phase of IrTe₂ and, in the process, clarify the origin of structural instability in this layered material. What differentiates this work from prior efforts [7] are the higher energy scans and c -polarized measurements, the combination of which provides evidence for the parity-allowed bonding-antibonding transition within the d_{xy} orbital of the Ir dimers in the 1/5th state. Interband transitions from the mixed Ir/Te bands into the d_{xy} antibonding orbital are also identified in the charge ordered phase. Analysis of these features reveals the primary role of iridium rather than tellurium in determining the structural stability of the dimerized phase of IrTe₂. These findings deepen the understanding of charge order within the entire family of chalcogenides by providing insight into the interplay between local and itinerant physics. Whether similar ideas extend to single layer and tubular analogs is unclear at this time. They are, however, already useful for understanding other $4d$ - and $5d$ -containing van der Waals solids with extremely large lattice distortions.

High quality single crystals exposing the ab plane and c axis were grown using flux methods as described previously [1,8,13]. Near normal ab -plane and c -polarized reflectance measurements were performed using a series of spectrometers covering the 25 meV–6.4 eV energy range. The complex optical conductivity and other physical quantities were determined via Kramer-Kronig analysis of the reflectance [15]. DFT and DMFT calculations [16] were performed on a relaxed structure with the experimental dimerization imposed [11,12] using the charged self-consistent implementation of Ref. [17], based on the WIEN2K package [18], with spin-orbit coupling included [19,20].

Figures 2(a) and 2(c) display the Ir, Te, and orbitally resolved Ir d_{xy} partial densities of states (DOS) in the (1×1) and $(1/5, 0, 1/5)$ phases, respectively. In the (1×1) phase, both Ir and Te display diffuse metallic bands with Ir showing a pronounced maximum about 1.5 eV below the Fermi level. The band structure reveals numerous interband transitions between mixed Te(p) – Ir(d) states over a wide energy range [Fig. 2(b)]. In the $(1/5, 0, 1/5)$ state, the DOS displays more pronounced changes in the Ir-derived bands than Te [Fig. 2(c)]. This is especially true for the d_{xy} orbital, which is in the dimerization direction [21]. In analogy with the traditional chemical bonding problem in the H₂ molecule, distortion causes the d_{xy} orbital on the dimerized Ir to split. It develops a bonding orbital doublet centered at ≈ -2.5 eV and a corresponding unoccupied antibonding orbital at ≈ 0.6 eV. The predicted bandwidths are ≈ 0.5 –1.0 eV. This splitting is a consequence of Ir dimerization, in which some of the Ir-Ir bonds shorten from 3.9 to 3.1 Å [11,12]. The formation of deep bonding orbitals reduces (i) the overall system energy and (ii) the DOS at the Fermi level. This provides stability to the 1/5th phase. Importantly, the formation of such orbitals creates optically active interband excitations [11,12] that can be tested against measurements. The key optical excitations are shown in the band structure plots of Figs. 2(b) and 2(d). In the 1/5th phase, there are two specific transitions into the d_{xy} antibonding orbital. Parity-allowed transitions from d_{xy} bonding to d_{xy} antibonding orbitals are predicted to be in the visible energy range [dashed red lines, Fig. 2(d)]. Another

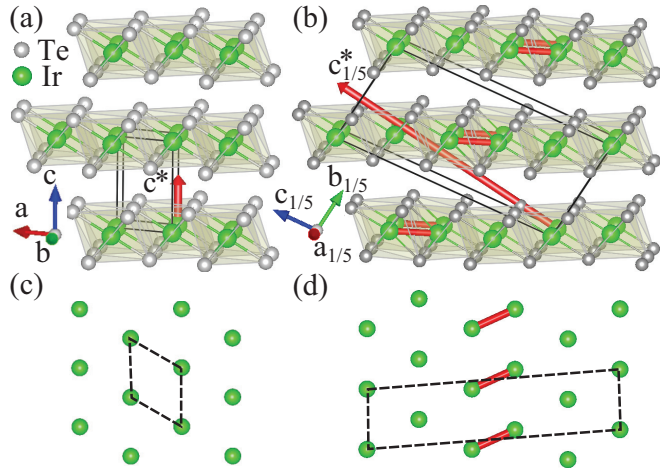


FIG. 1. (Color online) Crystal structure of IrTe₂ in the (a) high temperature (1 × 1) phase and (b) the low temperature (1/5,0,1/5) dimerized state [11,12]. The boxes depict crystallographic unit cells at 300 and 225 K, respectively. The crystallographic axes are shown with arrows. The reciprocal space axes c^* and $c_{1/5}^*$ are indicated. (c) and (d) display the triangular Ir layers. Dashed lines depict the projections of the appropriate unit cells on these layers. The Ir dimers, determined by experiment [11,12], are indicated with thick (red) lines in (b) and (d).

set of excitations originate from Ir(*d*)/Te(*p*) bands close to the Fermi level (near 0.8 eV, dashed blue). We discuss both excitations and their importance in the local dimerization process below.

Figure 3(a) displays the *ab*-plane reflectance at 300 and 225 K. These temperatures correspond to the high temperature (1 × 1) and high resistivity (1/5,0,1/5) phases, respectively [11,13]. Distinct temperature-induced reflectance changes are obvious from a casual inspection. The *ab*-plane spectra up to 3 eV is also in overall agreement with the work of Fang *et al.* [7], although as we shall see, the extra energy range of our investigation (along with the *c*-axis data) are invaluable. Figures 3(b) and 3(c) compare the theoretical and experimental *ab*-plane conductivities in the (1 × 1) and (1/5,0,1/5) phases, respectively [21]. The important optical transitions are indicated by solid and dashed lines. The agreement between theory and experiment is overall excellent, although the absolute optical conductivity values, the widths, and intensities differ somewhat [22]. In the (1 × 1) phase, all excitations take place between mixed Ir/Te bands and are of charge transfer type. The features centered at 2.5 eV have a particularly strong oscillator strength due to the high Ir/Te density of states 2 eV below the Fermi level and are common to both phases. The *c*-axis reflectance is shown in Fig. 3(d), and the optical conductivities of the two phases are presented in Figs. 3(e) and 3(f). Qualitatively, the *c*-axis spectra strongly resemble the *ab*-plane response.

Although the electronic structure of the (1/5,0,1/5) phase of IrTe₂ is complex, it is still possible to identify the optical excitations of interest. This is because the interband transitions in the 1/5th phase are significantly different from those in the (1 × 1) state. We have highlighted the three types of excitations that are characteristic of the distorted phase [Figs. 3(c) and 3(f)]. The lowest energy excitation at 0.5 eV (orange dashed

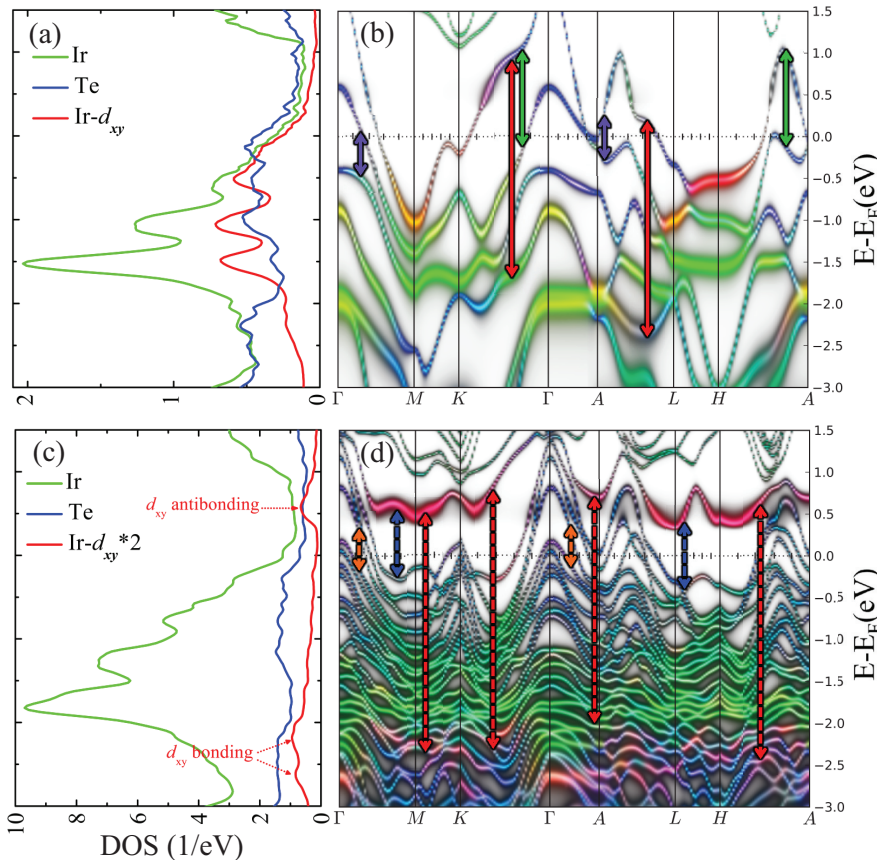


FIG. 2. (Color online) (a), (b) Ir, Te DOS and orbitally resolved Ir d_{xy} DFT-DMFT states of IrTe₂ in the (1 × 1) phase and the associated band structure. The spectral functions are color coded with projections of the Ir, Te, and Ir d_{xy} orbitals with green, blue, and red, respectively. Color mixing denotes band hybridization, which changes through the zone. The arrows denote excitations discussed in the text. (c), (d) The DOS in the (1/5,0,1/5) phase along with the corresponding band structure. The predicted formation of bonding and antibonding Ir orbitals in the (1/5,0,1/5) phase is shown in red [(c)]. Here, the Ir d_{xy} DOS is projected only to those Ir atoms which form dimers. The Ir d_{xy} orbital has lobes that point in the dimerization direction [21]. The excitations from the hybridized Ir/Te bands to the Ir d_{xy} antibonding state are indicated by the dashed blue arrows, and those related to the bonding-antibonding split are shown by the dashed red arrows (d).

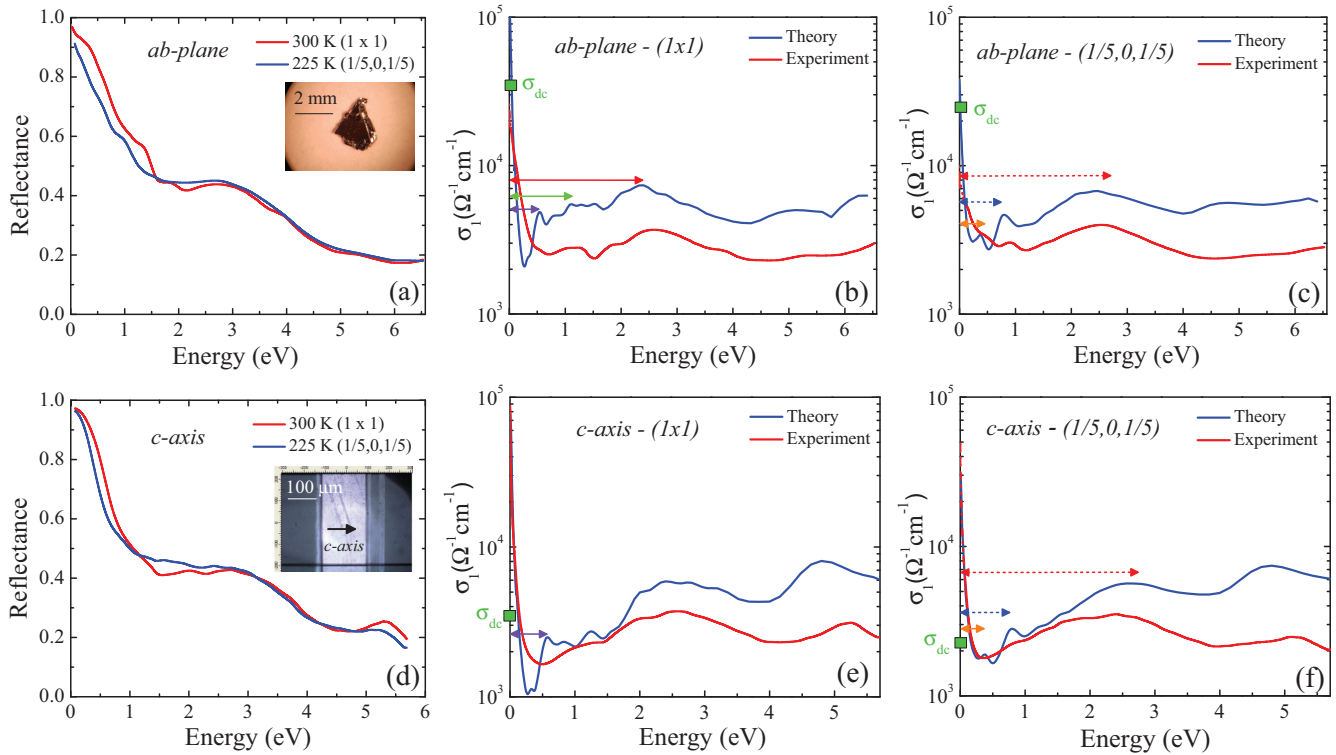


FIG. 3. (Color online) (a)–(c) *ab*-plane reflectance and optical conductivity of IrTe₂ in the (1 × 1) and (1/5,0,1/5) phases at 300 and 225 K, respectively. The inset in (a) shows a photograph of the *ab*-plane single crystal. (d)–(f) *c*-polarized reflectance and optical conductivity of IrTe₂ at 300 and 225 K. The inset shows a photograph of the crystal exposing the *c* axis with a knife edge aperture. The arrow indicates the *c*-axis direction, which corresponds to the (1 × 1) crystallographic axes. The dashed blue and red lines denote transitions into the Ir *d_{xy}* antibonding orbital from mixed Ir/Te and Ir *d_{xy}* bonding states, respectively. The dc conductivities from transport measurements are shown as green squares for comparison [8,13].

line) is charge transfer in nature. It is similar to what is seen in the (1 × 1) phase and does not reveal very much about Ir dimerization [23]. The excitations near 0.8 and 3 eV are different.

The transition predicted to be at approximately 0.8 eV (dashed blue line) originates from mixed Ir(*d*)/Te(*p*) bands close to the Fermi level transiting into the Ir *d_{xy}* antibonding orbital. This is one of the two excitations in the 1/5th state that can be traced directly to Ir dimer formation. According to theory, both the *ab*-plane and *c*-axis optical conductivities should have prominent peaks. Our measurements concur, although they reveal that the 0.8 eV excitation is broader than predicted. Moreover, a comparatively stronger feature is identified in the *ab*-plane data, only slightly blueshifted (by 0.1 eV) from the calculated value. We conclude that despite the challenges of a complex band structure, we are able to verify the presence of an excitation involving the Ir *d_{xy}* antibonding orbital in the absolute optical conductivity.

A direct transition from the bonding to antibonding orbital of Ir *d_{xy}* in the (1/5,0,1/5) phase is predicted to take place near 3 eV [dashed red line, Figs. 3(c) and 3(f)]. Perhaps not surprisingly, a clear signature of this excitation is challenging to uncover from the theoretical optical conductivity curve, due to the fact that it has a relatively small oscillator strength. This is because only the dimerized Ir *d_{xy}* electrons are involved, and there is an overall low concentration of dimers (one dimer for every five iridium atoms) [11]. At the same time, the

large background of mixed Ir-Te charge transfer excitations has a high joint density of states, completely overwhelming this modest feature. Taken together, the situation looks bleak, both in terms of unraveling the signature of the bonding to antibonding transition from the optical matrix element or uncovering it in the measured optical properties.

Direct evidence of the bonding to antibonding transition can, however, be obtained when the optical conductivity in the low temperature 1/5th phase is normalized by the high temperature (1 × 1) phase data. This methodology exposes clear differences between two phases while eliminating commonalities. Figure 4 displays the normalized *ab*-plane and *c*-axis spectra, respectively. The important optical transitions in the 1/5th phase are immediately apparent in both theory and experiment. The large theoretical peak at 0.8 eV that emanates from transitions between Ir/Te bands to *d_{xy}* antibonding levels (peak 2) can be assigned to the strong experimental features at 0.9 and 0.7 eV in the *ab*-plane and *c*-axis data, respectively. In the same spirit, the theoretical doublet centered near 2.8 eV [11,12] that corresponds to excitations between bonding and antibonding *d_{xy}* levels (peak 5) can be assigned to the experimental doublet centered close to 2.9 eV in the *ab* plane and 3.0 eV along the *c* axis. The doublet separations in peak 5 are about 0.5 eV, on the order of the DOS splitting in the bonding orbital [Fig. 2(c)]. Thus, we find evidence for transitions to the *d_{xy}* antibonding orbital in the absolute spectra as well as the ratio spectra. Evidence for the *d_{xy}* bonding

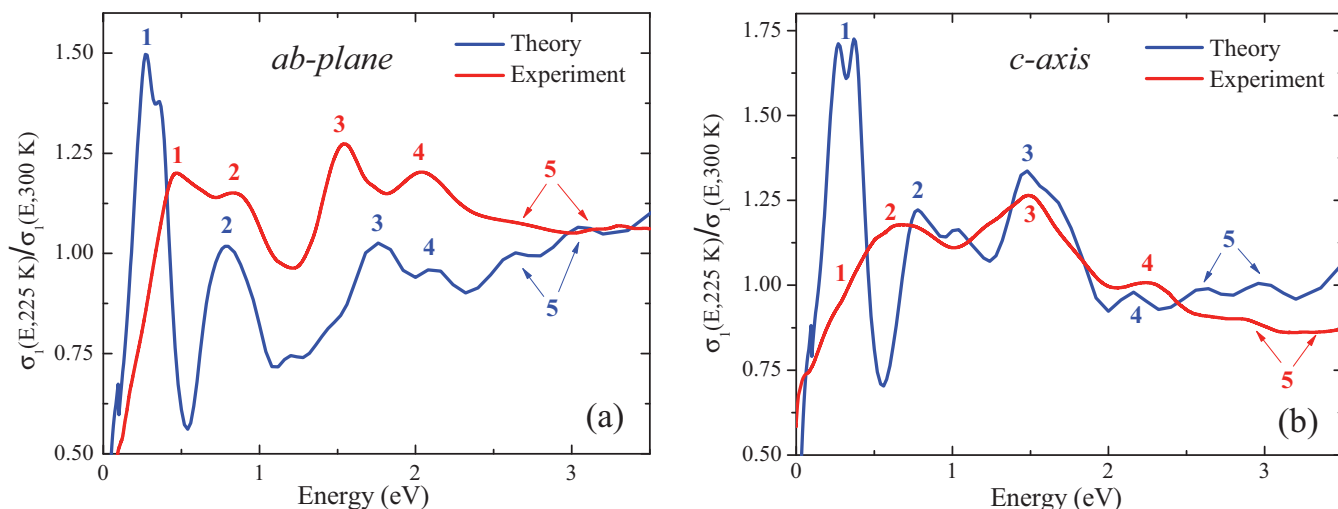


FIG. 4. (Color online) Experimental (red) and theoretical (blue) optical conductivity in the $(1/5,0,1/5)$ phase normalized by the high temperature phase data in the (a) *ab*-plane and (b) *c*-axis direction. This rendering reveals differences between the two phases and eliminates commonalities. The mixed Ir/Te-Ir d_{xy} antibonding excitation (peak 2) and bonding-antibonding splitting (peak 5) are revealed in the ratio spectra, both in the *ab* plane and along the *c* axis.

to antibonding transition is found only in the conductivity ratio spectra. Peaks 1, 3, and 4 are large oscillator strength transitions between mixed Ir/Te bands [23].

The confirmation of bonding-antibonding splitting demonstrates that Ir plays the dominant role in stabilizing the low temperature phase of IrTe₂. In particular, the formation of the d_{xy} bonding orbital reduces the system energy and stabilizes the low symmetry structure of IrTe₂ over the high symmetry state. In other words, the occupation of the Ir bonding orbital provides stability to the 1/5th phase. Tellurium plays a secondary role by adjusting to Ir dimerization through elastic coupling [11]. In fact, it can be argued that Te prevents dimerization among all iridium atoms as the gain in electronic energy is offset by the increase in elastic energy. Spin-orbit coupling, somewhat unexpectedly, is less important here, unlike many other iridates [24].

To summarize, we combined optical spectroscopy and complementary electronic structure calculations to uncover d_{xy} bonding-antibonding splitting in IrTe₂ due to dimerization of Ir centers. This local, rather than itinerant, physics is revealed by two excitations into the unoccupied d_{xy} antibonding orbital,

one originating from mixed Ir/Te bands close to Fermi level and the other from the deeper bonding d_{xy} orbital. These spectral signatures, in combination with simple energy arguments, establish the dominant role of iridium (rather than tellurium) in triggering the $(1/5,0,1/5)$ structural instability. Although the question of local versus itinerant origin of the charge order in IrTe₂ is resolving in favor of the former, this is an open question in other chalcogenides, especially those containing 4d and 5d centers and substantial spin-orbit coupling. The connection between the properties of the 1/5th phase of IrTe₂ and the development of the lower temperature 1/6, 1/8, and 1/11 phases will be explored in forthcoming work.

All authors acknowledge NSF-DMREF (DMR-1233118) for support of this research. G.L.P. was supported by NSF DMR-1004568. Work at Postech was funded by the Max Planck Postech/Korea Research Initiative Program (2011-0031558) through the National Research Foundation of Korea funded by the Ministry of Education, Science and Technology. We thank Weida Wu and David Vanderbilt for useful discussions.

- [1] J. J. Yang, Y. J. Choi, Y. S. Oh, A. Hogan, Y. Horibe, K. Kim, B. I. Min, and S.-W. Cheong, *Phys. Rev. Lett.* **108**, 116402 (2012).
- [2] S. Jobic, P. Deniard, R. Brec, J. Rouxel, A. Jouanneaux, and A. N. Fitch, *Z. Anorg. Allg. Chem.* **598**, 199 (1991).
- [3] N. Matsumoto, K. Taniguchi, R. Endoh, H. Takano, and S. Nagata, *J. Low Temp. Phys.* **117**, 1129 (1999).
- [4] B. Sipoš, A. F. Kusmartseva, A. Akrap, H. Berger, L. Forro, and E. Tutis, *Nat. Mater.* **7**, 960 (2008).
- [5] A. F. Kusmartseva, B. Sipoš, H. Berger, L. Forro, and E. Tutis, *Phys. Rev. Lett.* **103**, 236401 (2009).
- [6] D. Ootsuki, S. Pyon, K. Kudo, M. Nohara, M. Horio, T. Yoshida, A. Fujimori, M. Arita, H. Anzai, H. Namatame, M. Taniguchi, N. L. Saini, and T. Mizokawa, *J. Phys. Soc. Jpn.* **82**, 093704 (2013).
- [7] A. F. Fang, G. Xu, T. Dong, P. Zheng, and N. L. Wang, *Sci. Rep.* **3**, 1153 (2013).
- [8] Y. S. Oh, J. J. Yang, Y. Horibe, and S.-W. Cheong, *Phys. Rev. Lett.* **110**, 127209 (2013).
- [9] D. Ootsuki, Y. Wakisaka, S. Pyon, K. Kudo, M. Nohara, M. Arita, H. Anzai, H. Namatame, M. Taniguchi, N. L. Saini, and T. Mizokawa, *Phys. Rev. B* **86**, 014519 (2012).
- [10] H. Cao, B. C. Chakoumakos, X. Chen, J. Yan, M. A. McGuire, H. Yang, R. Custelcean, H. Zhou, D. J. Singh, and D. Mandrus, *Phys. Rev. B* **88**, 115122 (2013).
- [11] G. L. Pascut, K. Haule, M. J. Gutmann, S. A. Barnett, A. Bombardi, S. Artyukhin, T. Birol, D. Vanderbilt, J. J. Yang, S.-W. Cheong, and V. Kiryukhin, *Phys. Rev. Lett.* **112**, 086402 (2014).

- [12] T. Toriyama, M. Kobori, T. Konishi, Y. Ohta, K. Sugimoto, J. Kim, A. Fujiwara, S. Pyon, and K. Kudo, and M. Nohara, *J. Phys. Soc. Jpn.* **83**, 033701 (2014).
- [13] P.-J. Hsu, T. Maurer, M. Vogt, J. J. Yang, Y. Seok Oh, S.-W. Cheong, M. Bode, and W. Wu, *Phys. Rev. Lett.* **111**, 266401 (2013).
- [14] S. Pyon, K. Kudo, and M. Nohara, *J. Phys. Soc. Jpn.* **81**, 053701 (2012).
- [15] F. Wooten, *Optical Properties of Solids* (Academic, New York, 1972).
- [16] G. Kotliar, S. Y. Savrasov, K. Haule, V. S. Oudovenko, O. Parcollet, and C. A. Marianetti, *Rev. Mod. Phys.* **78**, 865 (2006).
- [17] K. Haule, C.-H. Yee, and K. Kim, *Phys. Rev. B* **81**, 195107 (2010).
- [18] P. Blaha, K. Schwartz, G. Madsen, D. Kvasnicka, and J. Luitz, *WIEN2k: An Augmented Plane Wave + LO Program for Calculating Crystal Properties* (TU Wien, Vienna, 2001).
- [19] H. Zhang, K. Haule, and D. Vanderbilt, *Phys. Rev. Lett.* **111**, 246402 (2013).
- [20] J. P. Perdew, K. Burke, and M. Ernzerhof, *Phys. Rev. Lett.* **77**, 3865 (1996).
- [21] Both the crystallographic and local coordinates were selected to allow the strongest comparison between theory and experiment. The theoretical *ab*-plane and *c*-axis analysis is along the high temperature (1×1) crystallographic axes [Fig. 1(a)] in both the high and low temperature phases for consistency with the measured optical properties. We also choose a local coordinate system on the Ir centers such that the lobes of the d_{xy} orbital point in the direction of the dimer bond. This orbital alignment allows the electronic structure changes due to Ir dimerization to be projected into the Ir d_{xy} orbital. The dimer bonds are shown by thick red lines in Fig. 1.
- [22] Quantitative discrepancies can be rationalized as follows: First, material-specific theoretical predictions have several built-in assumptions, even though we have used some of the most sophisticated electronic structure methods available (DFT-DMFT). Second, optical conductivity calculations involve a choice of broadening factors. This choice obviously influences the perceived agreement between theory and experiment. Finally, theory does not account for roughness or irregularities in a real material. Such factors generally lower the optical conductivity and broaden the features, although we routinely correct for scattering issues with an aluminum overcoat.
- [23] The lowest energy transition (0.5 eV, dashed orange) is between mixed Ir(*d*)/Te(*p*) states, similar to what is seen in the (1×1) phase. Peak 1 appears clearly as a shoulder on the Drude peak of the *ab*-plane spectrum but is obscured due to broadening along *c*. This feature is charge transfer in nature (as peaks 3 and 4) and does not reveal very much about dimerization.
- [24] B. J. Kim, H. Jin, S. J. Moon, J.-Y. Kim, B.-G. Park, C. S. Leem, Jaejun Yu, T. W. Noh, C. Kim, S.-J. Oh, J.-H. Park, V. Durairaj, G. Cao, and E. Rotenberg, *Phys. Rev. Lett.* **101**, 076402 (2008).